

EdgeStereo: A Context Integrated Residual Pyramid Network for Stereo Matching

Xiao Song, Xu Zhao, Hanwen Hu, Liangji Fang

Shanghai Jiao Tong University

Abstract. Recently convolutional neural network (CNN) promotes the development of stereo matching greatly. Especially those end-to-end stereo methods achieve best performance. However less attention is paid on encoding context information, simplifying two-stage disparity learning pipeline and improving details in disparity maps. Differently we focus on these problems. Firstly, we propose an one-stage context pyramid based residual pyramid network (CP-RPN) for disparity estimation, in which a context pyramid is embedded to encode multi-scale context clues explicitly. Next, we design a CNN based multi-task learning network called EdgeStereo to recover missing details in disparity maps, utilizing mid-level features from edge detection task. In EdgeStereo, CP-RPN is integrated with a proposed edge detector HED_{β} based on two-fold multi-task interactions. The end-to-end EdgeStereo outputs the edge map and disparity map directly from a stereo pair without any post-processing or regularization. We discover that edge detection task and stereo matching task can help each other in our EdgeStereo framework. Comprehensive experiments on stereo benchmarks such as Scene Flow and KITTI 2015 show that our method achieves state-of-the-art performance.

Keywords: stereo matching, context pyramid, residual pyramid, edge detection, multi-task learning

1 Introduction

Stereo matching is indispensable for robotics and autonomous driving [34,1]. Given a rectified stereo pair, a stereo algorithm aims at finding correspondence of each pixel between two images. A popular four-step pipeline [33] includes matching cost computation to measure the similarity of two pixels of two images, cost aggregation to smooth matching cost in neighborhood, disparity calculation to predict initial disparity from cost volume and finally disparity refinement.

Traditional stereo methods, patch based CNN models and end-to-end disparity networks are three categories of stereo algorithms. Traditional methods [15,42] are well studied following stereo pipeline, whose performance is limited.

Since Zbontar and LeCun [41] first introduce CNN to calculate matching cost, most of patch based stereo methods [7,25] focus on using CNN to generate unary terms. Though performance on several benchmarks [10,28,32] is improved, these methods suffer from severe limitations: (i) Limited receptive field. (ii) The usage of shallow, hand-crafted regularization and post-processing functions.

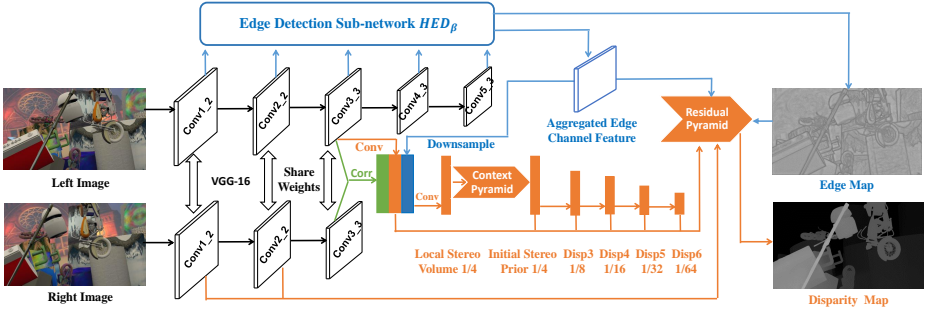


Fig. 1: The overview of our proposed EdgeStereo, where HED_{β} and CP-RPN are integrated sharing the VGG-16 backbone. Given a stereo pair, the edge map and disparity map are output simultaneously. (i) Our edge network HED_{β} is shown in blue and the rest denotes disparity network CP-RPN. (ii) The calculation of matching cost is shown in green. Context pyramid and encoder-decoder are shown in orange. The encoder contains 4 blocks from “Disp3” to “Disp6”, where each block consists of 2 convolutional layers and halves the resolution. Detailed structures of context pyramid and decoder (residual pyramid) are displayed in Fig. 2 and Fig. 3 respectively.

Currently end-to-end stereo methods [27,18,30] achieve state-of-the-art performance. For instance, CRL [30] cascades a disparity refinement network on DispNet [27] to refine the initial disparity map. 3D convolutions are employed in GC-Net [18] to learn disparity maps directly from specifically designed feature volume. However drawbacks still exist: (i) Semantical context information isn’t encoded explicitly for ill-posed regions, such as occlusions and textureless regions. (ii) Experiments in Section 4 reveal that multi-stage refinement structures [30,11] are not efficient. (iii) High-dimensional feature volume based 3D convolution in [18,40] is computationally expensive.

To break aforementioned limitations, we propose an end-to-end context pyramid based residual pyramid network (CP-RPN) for disparity estimation. It comes up with two spotlights: (i) An embedding context pyramid. (ii) A residual pyramid for learning and refining the disparity map in a single encoder-decoder. Hence, our CP-RPN is an one-stage disparity network with no need for cascaded refinement networks or complex multi-stage training.

Undoubtedly, stereo matching will benefit from semantical context cues, especially for ill-posed regions. However, utilizing a single-scale context cue can’t encode context for objects with arbitrary sizes and may cause over-smoothing. Hence encoding both local priors and multi-scale context cues is crucial for stereo matching. The pyramid structure is proven effective for encoding multi-scale information. Recent successful pyramids own heavy computational burdens [21,9,43], contrarily we design a simple but effective context pyramid.

To facilitate learning dense disparity maps, we borrow the idea of “From Easy to Tough” in curriculum learning [3]. In other words, learning at the smallest scale is easiest and learning residual is easier than direct regression as indicated

in ResNet [14]. Hence the multi-scale decoder is formulated as a residual pyramid in our CP-RPN with three features: (i) A smallest-scale disparity map is directly learned at the bottom of residual pyramid. (ii) For other scales, a residual map is learned for refinement then added to a coarse disparity map upsampled from previous scale, obtaining a larger and refined disparity map. (iii) At each scale besides the smallest, right image is downsampled then warped according to the upsampled disparity map from previous scale, obtaining a synthesized left image. Error map between the synthesized and real left images is utilized as a geometric constraint for learning the residual map at each scale.

However, the introduced CP-RPN inevitably lose some subtle details in the disparity map, due to the lack of mid-level features after too much forward propagation. Hence we resort to the multi-task learning framework to obtain extra mid-level information from other visual cues. The edge detection task is a suitable choice because the edge map is usually learned from mid-level representations. Hence we design an end-to-end edge network called HED_{β} based on the baseline model HED [38], in which the shared “aggregated edge channel feature” is constructed for multi-task interactions. Finally we integrate HED_{β} and CP-RPN into an end-to-end multi-task network called EdgeStereo. The interactions between two tasks in EdgeStereo are two-fold: (i) The aggregated edge channel feature is downsampled to varied sizes through a differentiable interpolation layer, then concatenated at the corresponding scale in residual pyramid. (ii) The edge map output from HED_{β} is also downsampled to varied sizes, serving as a regularization prior for learning disparity or residual map at corresponding scale. The overview of EdgeStereo is shown in Fig. 1.

In EdgeStereo, multi-task learning is conducted based on a multi-stage training strategy. After the joint learning of two tasks, EdgeStereo outperforms the original CP-RPN on stereo matching task in both quantitative and qualitative aspects. Surprisingly, the edge map output from HED_{β} is also refined. Due to the fact that ground-truth edge maps are not provided in stereo datasets, we can only evaluate the outputting edge map qualitatively.

In summary, our contributions are three-fold. (i) We design a novel one-stage network for stereo matching, in which a context pyramid and a residual pyramid are embedded. (ii) We are the first to integrate stereo matching with edge detection task into a CNN based multi-task architecture. In our EdgeStereo, two tasks can help each other. (iii) State-of-the-art performance is achieved on standard stereo benchmarks: Scene Flow [27] and KITTI 2015 [28].

2 Related Work

Stereo Matching. We hereby review stereo matching with focus on state-of-the-art CNN based, non-end-to-end or end-to-end stereo methods.

Among non-end-to-end deep stereo algorithms, each step in stereo pipeline could be replaced with a CNN model. For example, Luo *et al.* [25] trains a simple multi-label classification network for matching cost computation. Shaked and Wolf [37] introduce an initial disparity calculation network pooling global

information from the cost volume. Gidaris *et al.* [11] substitute the handcrafted disparity refinement methods with a three-stage refinement network.

As for end-to-end deep stereo algorithms, all steps in the stereo pipeline are integrated for joint optimization. To enable the training of an end-to-end disparity network, Mayer *et al.* [27] create a large synthetic dataset, meanwhile they also propose a baseline model called DispNet with an encoder-decoder structure. Based on DispNet, Pang *et al.* [30] cascade a residual learning (CRL) network for further refinement. Different from DispNet, Kendall *et al.* [18] propose the 3-D convolution based GC-Net. Based on GC-Net, Yu *et al.* [40] add an explicit cost aggregation structure. An unsupervised method is proposed in [44]. Our CP-RPN is also an end-to-end network, but we explicitly model context cues for stereo matching and our one-stage encoder-decoder is powerful and efficient.

Incorporating Stereo Matching with Other Tasks. Undoubtedly, stereo matching will benefit from the helpful cues or features from other tasks. For example, Bleyer *et al.* [4] first conduct joint stereo matching and object segmentation. Guney and Geiger [13] propose a method called Displets, utilizing foreground object recognition to help stereo matching. More vision tasks are fused through a slanted plane in [39]. However, these traditional and hand-crafted multi-task methods are not robust. To our knowledge, our EdgeStereo is the first CNN based multi-task structure to help stereo matching.

Edge Detection. To further refine the disparity estimation, we resort to the edge detection task for mid-level representations. Inspired by FCN [24], Xie *et al.* [38] design the first end-to-end edge detection network called holistically-nested edge detector (HED) based on VGG-16 net. Recently, Liu *et al.* [23] modify the structure of HED, combining richer convolutional features from VGG body. These end-to-end edge networks can be easily incorporated with CP-RPN.

Deep Learning Based Multi-task Structure. Cheng *et al.* [8] propose the SegFlow, an architecture for the joint learning of video object segmentation and optical flow. However, this architecture requires training data containing all types of labels. Mao *et al.* [26] also propose a multi-task architecture called HyperLearner to help pedestrian detection. Diverse channel feature networks provide various features to be concatenated with backbone detection network. However, in HyperLearner, outputs from other tasks aren't utilized and varied tasks can't help each other. Our EdgeStereo successfully breaks these limitations.

3 Approach

For better illustration, in this section, we will first introduce the original CP-RPN for disparity estimation. Afterwards we will introduce our end-to-end multi-task learning architecture EdgeStereo, including descriptions of HED_β network and interactions between CP-RPN and HED_β .

3.1 Context Pyramid Based Residual Pyramid Network (CP-RPN)

Our end-to-end CP-RPN consists of three components: local stereo volume extraction, context pyramid and the 2-D encoder-decoder (residual pyramid).

Local Stereo Volume Extraction. First we learn the deep representation for matching cost calculation. Unary feature extraction module is usually a siamese structure with two shared-weight towers. For the following two reasons, we employ a part of VGG-16 backbone pretrained on ImageNet [20] as each unary feature extraction tower: extracted features are proven robust for many vision tasks [24,31] and in this way CP-RPN can be easily integrated with HED_β . To compromise between detailed correspondence and large receptive field, we only use conv1_1 to conv3_3 from VGG-16. As shown in Fig. 1, the output of the first tower conv3_3a is the unary feature map for the left image and the second tower outputs conv3_3b for the right image.

1-D Correlation with a max displacement of 50 is performed between conv3_3a and conv3_3b, obtaining a cost volume capturing coarse correspondence between the stereo pair. The cost volume and two unary feature maps are all at quarter the resolution of the input. Then an 1×1 convolution with halved output channels is applied to conv3_3a, in order to extract reduced but refined unary features from the left image then concatenated with cost volume. Afterwards the concatenation is convolved with another 1×1 kernel, obtaining the **local stereo volume**. By this formulation, we intend to provide both local semantic features and local correspondence distributions for the following context pyramid.

Context Pyramid. Considering a big textureless wall, many potential correspondences exist for each pixel if only based on local inference. Hence global context cues are necessary. However a single-scale context representation is not sufficient for stereo matching. A scene contains objects with arbitrary sizes and an end-to-end disparity network should infer correspondences for all of them simultaneously. If only the large-scale context cues are utilized, small objects are likely to be overlooked. Contrarily disparities of big stuff might be inconsistent or discontinuous based on small-scale context cues only. Hence proposed context pyramid aims at capturing multi-scale context cues in a simple manner.

Moreover, if we only utilize global priors, the disparity map will be excessively smooth without fine-grained details. For instance, supposed jumps in disparity won't appear when coinciding with strong image gradients. Hence combing multi-scale context cues with local priors is beneficial.

Obtained local stereo volume provides adequate information for capturing context cues, hence context pyramid is applied on it. Our context pyramid is formulated as a module with four parallel branches corresponding to four pyramid levels. The top of the context pyramid corresponds to the largest context scale. As mentioned in [43], the size of receptive field roughly indicates how much we use context. Hence each branch in the pyramid is designed with a different receptive field to capture context cues at corresponding scale. Afterwards, four outputs from different branches are concatenated as the multi-scale context cues. Because the local stereo volume also serves as the local priors, finally we concatenate it with the multi-scale context cues, obtaining the **initial stereo prior** as the input of the 2-D encoder-decoder structure.

As shown in Fig. 2, each branch in context pyramid consists of two or three layers followed by a ReLU each. The channel number of the first layer is 256, then

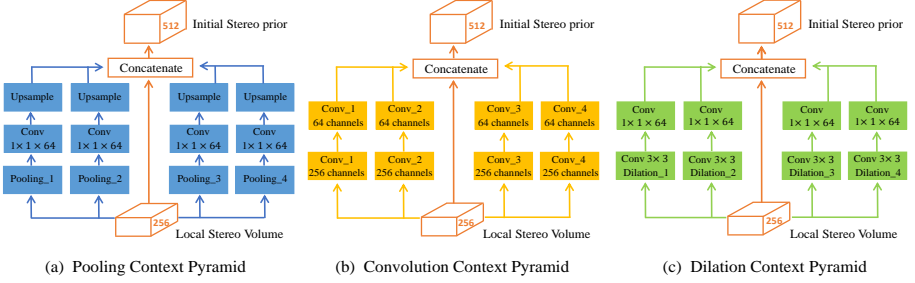


Fig. 2: Structures of Pooling, Convolution and Dilation Context Pyramids. Each Pyramid contains 4 branches representing 4 pyramid levels. The local stereo volume is also concatenated. In each pyramid, the leftmost branch encodes the largest-scale context cues, so it corresponds to the top pyramid level with a subscript $_1$. The rightmost branch ($_4$) is at the bottom of the context pyramid, encoding the smallest-scale context cues. The input local stereo volume has 256 channels and the output initial stereo prior has 512 channels.

it’s reduced by 4 times in the second layer. Convolution, pooling and dilation [6] are three mainstream methods to enlarge the receptive field, hence three kinds of context pyramid are designed correspondingly.

(i) Convolution context pyramid. Each branch consists of two conv layers with a same kernel size. The kernel size decreases linearly from top to bottom. For example, 7×7 , 5×5 , 3×3 and 1×1 for each branch, denoted as $C\text{-}7.5.3.1$.

(ii) Pooling context pyramid. The first layer is an average pooling layer with varied pooling kernels. Bin size of pooling output increases from top to bottom. For example, 1×1 , 2×2 , 4×4 and 8×8 , denoted as $P\text{-}1.2.4.8$. The second layer is an 1×1 conv layer, then the bilinear interpolation is applied on each branch so that each output is at the same size of the local stereo volume.

(iii) Dilation context pyramid. Inspired by [6], the first layer is a 3×3 dilated conv layer, with a dilation decreasing from top to bottom. For example, 6, 3, 2 and 1, denoted as $D\text{-}6.3.2.1$. Similarly the second layer is an 1×1 conv layer.

In Section 4.2, we conduct further experiments to compare different context pyramids and the best is embedded in our CP-RPN.

Encoder-Decoder (Residual Pyramid). In order to replace the multi-stage refinement structure, we design a different encoder-decoder so that disparity learning and refinement can be fused into a single network.

Taking the initial stereo prior as input, the encoder contains four groups of conv layers. Each group consists of two 3×3 convolutions with strides of 2 and 1 respectively, resulting in a total downsampling factor of 64.

The decoder is formulated as a residual pyramid inspired by curriculum and residual learning [3,14]. Corresponding to the encoder, the decoder has seven available scales ($\frac{1}{64}$, $\frac{1}{32}$, $\frac{1}{16}$, $\frac{1}{8}$, $\frac{1}{4}$, $\frac{1}{2}$ and $1 \times$ of the input size). Learning at the smallest scale is easiest because output size is small and few details are needed. In addition, seven scales of the decoder make the multi-step curriculum learning possible. More specifically, we learn a simple disparity map at the $\frac{1}{64}$ scale, then

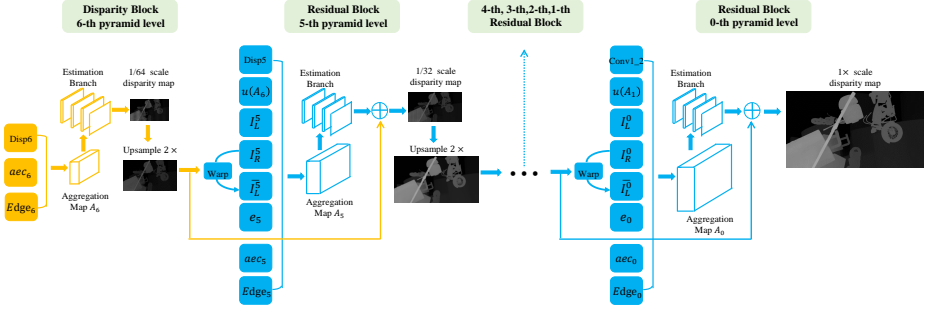


Fig. 3: Architecture of our residual pyramid, which contains a disparity block and six residual blocks. Working principles of six residual blocks are same, hence we only draw two residual block at the 5-th and 0-th pyramid levels. Disp6, Disp5 are from the encoder, aec_i and $Edge_i$ denote the aggregated edge channel feature and the edge map downsampled by a factor by 2^i . Other symbols are defined in the text. Finally, a disparity map at full resolution is output.

it's continuously upsampled and refined with residual maps at larger scales, until the largest scale where the refined disparity map at full resolution is output.

Based on this idea, the residual pyramid is proposed (Fig. 3), containing one disparity and six residual blocks. Seven blocks correspond to seven scales in residual pyramid. Hence our residual pyramid is inverted that the bottom of the pyramid corresponds to the smallest output scale. Disparity block is placed bottommost to learn the $\frac{1}{64}$ scale disparity map, while each upper residual block predicts the residual map at corresponding scale.

Let $K + 1$ denotes total scale numbers in residual pyramid ($K = 6$ here), so K -th scale denotes the smallest scale, $\{B_K, \dots, B_0\}$ denote all blocks from bottom to top (B_K denote disparity block). Let I_L and I_R denote left and right images, $u(\cdot)$ denote upsampling by a factor of 2 through a differentiable interpolation layer similar to the sampler module in STN [16], d_k and r_k denote disparity and residual map at the k -th scale ($0 \leq k \leq K$) respectively. Each block contains an aggregation map and an estimation branch.

Each aggregation map, denoted as A_k , is used for estimating the disparity or residual map. Aggregation map in the disparity block is the final output from encoder. However in each residual block, it is the concatenation of a skip-connected activation map from the encoder or VGG-16 backbone, upsampled aggregation map $u(A_{k+1})$ and geometric constraints. To fully utilize the epipolar geometry, at the k -th ($k \neq K$) scale in residual pyramid, I_L and I_R are first downsampled by a factor of 2^k as I_L^k and I_R^k . We then warp the I_R^k according to the upsampled disparity map from the previous scale $u(d_{k+1})$, obtaining a synthesized left image:

$$\overline{I}_L^k(x, y) = I_R^k(x - u(d_{k+1})(x, y), y) \quad (1)$$

The error map $e_k = |I_L^k - \overline{I}_L^k|$ is a heuristic geometric cue for learning the residual map. When considering HED $_{\beta}$, aggregated edge channel feature and edge map are also concatenated to A_k .

Taking the aggregation map as input, each estimation branch consists of four 3×3 conv layers. Each conv layer is followed by a ReLU layer, except the last conv layer with a single output channel. The estimation branch in B_K outputs d_K while other branches output r_k . The summation of r_k and upsampled disparity map from previous scale leads to a refined disparity map at scale k :

$$d_k = u(d_{k+1}) + r_k, 0 \leq k < K \quad (2)$$

Deep Supervised L1 Loss. Deep supervision can help stabilize training and improve performance [38], so we compute the l_1 loss between the disparity estimate and ground-truth disparity at each scale. At the k -th scale, let gt_k denote the ground-truth disparity map downsampled and scaled by a factor of 2^k , h_k and w_k denote corresponding height and width. Loss weight α_k for each scale is set to 1, hence the deep supervised l_1 loss is denoted as:

$$L_1^{total} = \sum_{k=0}^K \alpha_k \sum_{(x_k, y_k) \in d_k} \frac{1}{h_k \times w_k} |d_k(x_k, y_k) - gt_k(x_k, y_k)| \quad (3)$$

3.2 EdgeStereo

Edge Detection Network HED_β . Considering that edge map is usually learned from mid-level representations, hence these mid-level features are beneficial for learning details. FCN-based HED [38] outputs more semantically meaningful edge maps than traditional detectors [5]. However obtaining adequate edge channel features from HED is not easy. Mao *et al.* [26] add more conv layers but abandon the output layer in each side branch. They aggregate multi-level feature maps for a single output. In this way, edge detection becomes sensitive because deep supervision isn't used for training. In addition, crude feature aggregation in [26] may cause difficulty in convergence.

Meaningful edge channel features are obtained in condition that the output edge map is robust. Hence the major architecture of HED is preserved. The body network of our HED_β is the VGG-16 backbone from conv1_1 to conv5_3 pre-trained on ImageNet. We design five side branches starting from layer conv1_2, conv2_2, conv3_3, conv4_3 and conv5_3 respectively. Each branch consists of two 3×3 conv layers with 64 channels, a deconv layer to upsample the feature map at the full resolution, and an 1×1 conv layer to output the edge probability map. In the end, five edge probability maps are fused through an 1×1 conv layer (fusion layer), obtaining the final edge map.

To train HED_β , deep supervision is utilized where all side branches and the final fusion layer are supervised. We use a modified class-balanced cross-entropy loss, called "Annotator-robust Loss Function" in [23].

Interactions Between CP-RPN and HED_β . In EdgeStereo, the interactions between two networks are two-fold:

(i) Firstly, we construct the shared edge channel feature from HED_β . We first concatenate all feature maps from each deconv layer in each side branch. Then an 1×1 conv layer with 128 channels is applied on the concatenation,

obtaining the aggregated edge channel feature denoted as aec . We believe that the mid-level aggregated edge channel feature encodes both detailed appearance and semantics without losing too much information.

By sharing the aec , CP-RPN can benefit from semantically meaningful edge representations that HED_β learns. More specifically, aec interacts with CP-RPN at the local stereo volume and residual pyramid. Firstly, aec is concatenated with the cost volume and unary feature map to form the new local stereo volume. Secondly, we propose a multi-scale concatenation method for aec . For the k -th scale in residual pyramid, aec is first downsampled by a factor of 2^k through the differentiable interpolation layer mentioned above, then it's convolved with an 1×1 convolutional kernel, obtaining a downsampled and reduced edge channel feature denoted as aec_k . Channels of aec_k ($0 \leq k \leq 6$) are $\{16, 16, 32, 48, 64, 96, 128\}$. Finally each aec_k is concatenated to aggregation map A_k at corresponding scale, to help learning disparity or residual map implicitly.

(ii) We utilize the output from HED_β to regularize the disparity estimation. Sophisticated regularizers [12] are based on the idea of “edge preserving”, but hand-crafted penalty functions aren't robust. We directly input the edge map to CP-RPN, to help learning the smoothness regularization implicitly. The edge map output from HED_β is downsampled to seven sizes through the differentiable interpolation layer mentioned above. Each downsampled edge map is also concatenated to the aggregation map at corresponding scale in residual pyramid.

Multi-stage Training Strategy. In order to conduct the multi-task learning for EdgeStereo, we propose a multi-stage training strategy where the training phase is split into three stages.

In the first stage, only HED_β is trained on an edge detection dataset. In detail, parameters of all ImageNet pretrained convolutional layers in VGG-16 backbone (conv1_1 to conv5_3) are fixed. In the second stage, we fix the weights of VGG-16 backbone (conv1_1 to conv5_3) and HED_β , then train the EdgeStereo network on a stereo dataset. In the third stage, all layers in EdgeStereo are jointly optimized on the same stereo dataset. The deep supervised l_1 loss in Eq. (3) is employed in the second stage and the third stage.

4 Experiments

Experimental settings and results are presented in this section. We show performance of the original CR-RPN and EdgeStereo on stereo benchmarks quantitatively and qualitatively, then compare with other state-of-the-art stereo methods. We also visualize the better output edge maps after multi-task learning.

4.1 Experimental Settings

Datasets. Three different publicly available datasets are used in our work:

(i) For stereo matching, Scene Flow [27] and KITTI 2015 [28] datasets are used. Scene Flow is a synthesised dataset with dense ground-truth disparities. It contains $4k$ testing images. We only use the FlyingThings3D subset containing

more than $22k$ stereo pairs for training. We perform the same screening as CRL [30] that we remove a disparity image and the stereo pair if more than 25% of its disparity values are larger than 300. KITTI 2015 are real-world datasets with sparse ground-truth disparities. KITTI 2015 consists of 200 training pairs and 200 testing pairs.

(ii) For HED_β in EdgeStereo, the edge dataset BSDS500 [2] containing 300 training and 200 test images is used. Consistent with [22,23], we mix augmented training data of BSDS500 with PASCAL VOC Context dataset [29] for training.

Training. Our methods are all implemented based on Caffe [17]. Our used data augmentations are as same as the augmentations in DispNet [27] and HED [38].

(i) Training the original CP-RPN. All models are optimized using the Adam method [19] with $\beta_1 = 0.9$, $\beta_2 = 0.999$. We employ “Multistep” learning strategy with a batch size of 3. For training on Scene Flow, the initial learning rate is set to 10^{-4} and then reduced by a half at the $500k$ -th, $700k$ -th and $800k$ -th iteration. The training stops at the $900k$ -th iteration. For fine-tuning on KITTI 2015, the initial learning rate is set to 2×10^{-5} then reduced by a half at the $30k$ -th, $80k$ -th iteration. The fine-tuning stops at the $100k$ -th iteration to lessen the problem of over-fitting. Since some ground-truth disparities are not available for KITTI datasets, they are neglected when computing the l_1 loss.

(ii) Multi-stage training of EdgeStereo. In the first stage, HED_β is trained on BSDS500 for $30k$ iterations, with a batch size of 12 and a learning rate of 10^{-7} which is divided by 10 at the $15k$ -th and $25k$ -th iteration. The second and third stages are all trained on Scene Flow with a batch size of 2. We train for $400k$ iterations with a fixed learning rate of 10^{-4} in the second stage. Afterwards, we train for $600k$ iterations with a learning rate of 10^{-4} which is halved at the $300k$ -th and $500k$ -th iteration in the third stage. KITTI fine-tuning for EdgeStereo is as same as the KITTI fine-tuning for the original CP-RPN.

Testing. For evaluation on two public stereo matching datasets, we use end-point-error (EPE), which is calculated as the average Euclidean distance between estimated and ground-truth disparity. We also use the percentage of disparities with their EPE larger than t pixels ($> tpx$), denoted as t -pixel error.

4.2 Ablation Studies for Stereo Matching Task

In this section, we will conduct several ablation experiments on the Scene Flow dataset to justify the effectiveness of our design choices for disparity estimation. We adopt the one-stage model DispFulNet [30] (a simple variant of the DispNetC [27]) as the baseline model. All experimental results are shown in Table 1.

Local Stereo Volume Extraction. To demonstrate its effectiveness, we replace the unary extraction part in DispFulNet with our extraction tower (a part of VGG-16 backbone), 3-pixel error is reduced from 8.61% to 6.83%. Next, we apply an 1×1 convolution on the concatenation of unary features and coarse correlations to form our LSV, 3-pixel error is further reduced to 6.70%. That is because, more semantically meaningful features are obtained from our unary feature extraction tower and the cushioning 1×1 convolution help fully fuse the local semantical representations and local matching distributions.

Table 1: Comparative results on the Scene Flow dataset for disparity estimation networks with varied settings. “LSV” denotes our local stereo volume.

Model	$> 3px(\%)$	EPE	Time(s)
Basic ablation studies			
DispFulNet [30] (unary feature + encoder-decoder)	8.61	1.75	0.07
Our unary feature + encoder-decoder in DispFulNet	6.83	1.38	0.14
LSV + encoder-decoder in DispFulNet	6.70	1.37	0.14
LSV + our encoder-decoder	5.96	1.28	0.19
LSV + P -2.4.8.16 + our encoder-decoder (CP-RPN)	5.33	1.15	0.19
LSV + P -2.4.8.16 + encoder-decoder in DispFulNet	5.95	1.28	0.13
Context pyramid comparisons			
CP-RPN with convolution pyramid C -7.5.3.1	5.85	1.26	0.24
CP-RPN with convolution pyramid C -9.7.5.3	5.70	1.21	0.26
CP-RPN with convolution pyramid C -11.9.7.5	5.79	1.23	0.28
CP-RPN with pooling pyramid P -1.2.4.8	5.61	1.19	0.22
CP-RPN with pooling pyramid P -2.4.8.16	5.33	1.15	0.19
CP-RPN with dilation pyramid D -6.3.2.1	5.81	1.24	0.23
CP-RPN with dilation pyramid D -12.9.6.3	5.52	1.17	0.24
CP-RPN with dilation pyramid D -24.18.12.6	5.88	1.26	0.24
One-stage vs multi-stage refinement			
LSV + P -2.4.8.16 + encoder-decoder in DispFulNet + DRR [11]	5.48	1.17	0.47
LSV + P -2.4.8.16 + encoder-decoder and refinement in CRL [30]	5.34	1.16	0.31
LSV + P -2.4.8.16 + our one-stage encoder-decoder	5.33	1.15	0.19
Benefits from Edge Detection			
CP-RPN with C -7.5.3.1	5.85	1.26	0.24
CP-RPN with C -7.5.3.1 + HED_{β}	5.44	1.16	0.32
LSV + D -6.3.2.1 + encoder-decoder in DispFulNet	6.31	1.33	0.17
LSV + D -6.3.2.1 + encoder-decoder in DispFulNet + HED_{β}	6.02	1.29	0.25
LSV + P -2.4.8.16 + our encoder-decoder	5.33	1.15	0.19
LSV + P -2.4.8.16 + our encoder-decoder + HED_{β} (EdgeStereo)	4.99	1.12	0.29

Context Pyramid. Firstly, we choose a context pyramid (P -2.4.8.16), then train a model consisting of our local stereo volume, the choosen context pyramid and the encoder-decoder of DispFulNet. Compared with the model without context pyramid, 3-pixel error is reduced from 6.70% to 5.95%. Furthermore, as shown in the “Context pyramid comparisons” part in Table 1, adopting other context pyramids can also lower the 3-pixel error. Hence we argue that multi-scale context priors are beneficial for dense disparity estimation.

Encoder-Decoder. We use a same encoder as DispFulNet while the decoder is formulated as our residual pyramid. To demonstrate its effectiveness, we train a model consisting of our local stereo volume extraction and our encoder-decoder. Compared with the model with the encoder-decoder in DispFulNet, 3-pixel error is reduced from 6.70% to 5.96%. This proves that regressing disparities at each scale directly is inferior to our multi-scale residual learning.

Finally we train a CP-RPN model composed of our local stereo volume, context pyramid P -2.4.8.16 and our encoder-decoder. It yields a 3-pixel error of 5.33% and an EPE of 1.15, outperforming baseline model by 3.28%/0.60.

Comparisons of Various Context Pyramids. For comparison, we train different CP-RPN with varied context pyramids. In Table 1, three convolution pyramids don’t work well, improving only 0.11%, 0.26% and 0.17% respectively, in terms of 3-pixel error compared with the model without a context pyramid. In addition, the large dilation is inferior. 3-pixel error of D -24.18.12.6 is 5.88% while

Table 2: Comparisons of stereo matching algorithms on the Scene Flow test set.

metric	SGM	SPS-st	MC-CNN	DRR	DispNet	DispFulNet	CRL	GC-Net	CA-Net	Edge Stereo
$> 3px$	12.54	12.84	13.70	7.21	9.67	8.61	6.20	7.20	5.62	4.99
EPE	4.50	3.98	3.79	-	1.84	1.75	1.32	-	-	1.12

it’s reduced to 5.52% for *D-12_9.6_3*. *P-2_4.8_16* performs the best, achieving a 3-pixel error of 5.33%. Hence we use *P-2_4.8_16* in our final CP-RPN.

Comparisons with Multi-stage Refinement. The superiority of our one-stage model CP-RPN is proven. Firstly we compare with the three-stage refinement structure DRR [11]. We replace our encoder-decoder with encoder-decoder in DispFulNet, then cascade three additional networks for refinement like [11]. As can be seen, CP-RPN outperforms it by 0.15% and is 2.3 times faster. Next we compare with two-stage CRL [30] method. We replace our encoder-decoder with a disparity network and a refinement network in [30]. Its performance is almost same with CP-RPN but our CP-RPN is faster and has less parameters.

Benefits from Edge Detection. When the disparity network is integrated with edge detection network HED_{β} , performance is further improved. To prove this, we conduct several experiments that different disparity models are integrated with HED_{β} . As can be seen, the performance of all models is improved and we also give visual demonstrations shown in Fig. 4. Finally, we adopt the best CP-RPN (with *P-2_4.8_16*) integrated with HED_{β} as our EdgeStereo model.

4.3 Comparisons with Other Stereo Methods

Scene Flow. Firstly we consider some non-end-to-end methods (with public codes), including SGM [15], SPS-St [39], MC-CNN-fst [41] and DRR [11]. Next, we consider the most advanced end-to-end models (with public codes or results in the paper), including DispNetC [27], DispFulNet [30], CRL [30], GC-Net [18] and CA-Net [40]. The comparisons are presented in Table 2, our end-to-end model achieves the best performance in terms of two evaluation metrics. As shown in Fig. 4, our EdgeStereo produces very sharp disparity estimates.

KITTI. We have trained our EdgeStereo on all training data of KITTI 2015, then submitted our results to KITTI online leaderboard. For evaluation on KITTI 2015, we use the 3-pixel error in background (D1-bg), foreground (D1-fg) or all pixels (D1-all) in non-occluded or all regions. The results are shown in Table 3. The leaderboard ranks all methods based on the D1-all metric in all regions. Clearly, our EdgeStereo achieves state-of-the-art performance on KITTI 2015. In Fig. 6, we present few qualitative results achieved by EdgeStereo on KITTI test set. It can be observed that our method produces detailed results.

Result Analysis. For KITTI 2015, although we achieve a state-of-the-art 3-pixel error of 2.99% and outperforms the baseline model DispNetC (4.34%) significantly, it’s slightly inferior than CRL (2.67%) and GC-Net (2.89%). However EdgeStereo outperforms CRL and GC-Net obviously on Scene Flow test set. We think this difference is mainly attributed to the fact that KITTI 2015 training set is too small (only 200 training images). Our EdgeStereo is a multi-task structure hence the capacity of our network is larger than previous stereo structures.

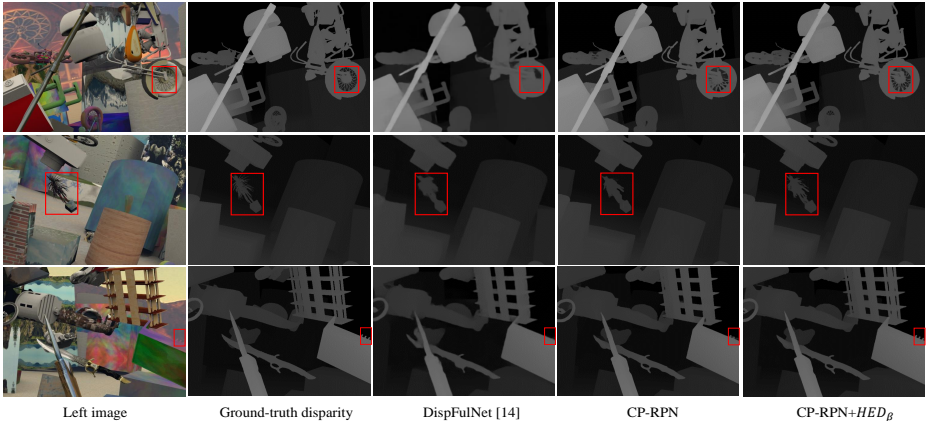


Fig. 4: Comparisons of different structures for stereo matching on Scene Flow dataset. In red boxes, EdgeStereo produces the sharpest disparity estimations.

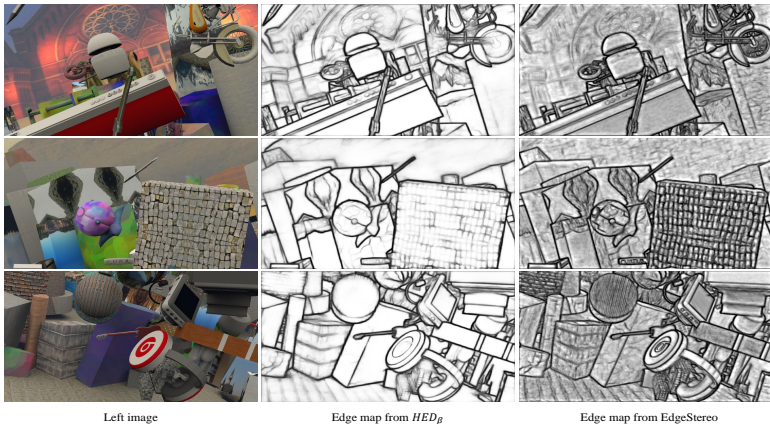


Fig. 5: Visual demonstrations of better edge map after joint learning with the disparity network CP-RPN. As can be seen, details in edge maps are improved significantly. All edge maps are not thinned by the non-maximum suppression.

The training data is required to be diverse enough when training such a complicated network with large capacity. However for KITTI, we can only finetune the EdgeStereo on such a small set. Undoubtedly the learning is not comprehensive and it’s somewhat over-fitted. If our EdgeStereo can “see” more scenarios during training, the performance should be much better. As can be seen, Scene Flow dataset contains more than 20 thousands training images, hence the well-learned EdgeStereo ranks the first among all stereo methods on this dataset.

4.4 Better Edge Map

Unfortunately, we can’t evaluate on stereo benchmarks whether the edge detection is improved after joint learning, because ground-truth edge map is not available in Scene Flow or KITTI 2015. Hence we only give visual demonstrations for better edge map. We conduct experiments on Scene Flow dataset shown

Table 3: Results on the KITTI 2015 stereo online leaderboard.

	All Pixels			Non-Occluded Pixels		
	D1-bg	D1-fg	D1-all↓	D1-bg	D1-fg	D1-all↓
CRL [30]	2.48	3.59	2.67	2.32	3.12	2.45
GC-Net [18]	2.21	6.16	2.87	2.02	5.58	2.61
EdgeStereo (ours)	2.70	4.48	2.99	2.50	3.87	2.72
DRR [11]	2.58	6.04	3.16	2.34	4.87	2.76
SsSMNet [44]	2.70	6.92	3.40	2.46	6.13	3.06
L-ResMatch [37]	2.72	6.95	3.42	2.35	5.74	2.91
Displets v2 [13]	3.00	5.56	3.43	2.73	4.95	3.09
PBCP [35]	2.58	8.74	3.61	2.27	7.71	3.17
SGM-Net [36]	2.66	8.64	3.66	2.23	7.44	3.09
MC-CNN-acrt [41]	2.89	8.88	3.88	2.48	7.64	3.33
DispNetC [27]	4.32	4.41	4.34	4.11	3.72	4.05

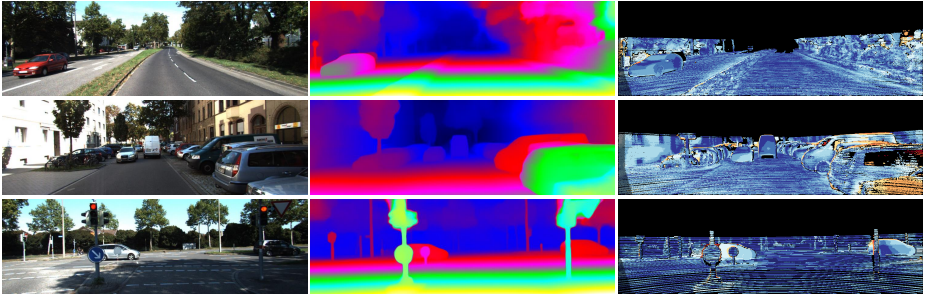


Fig. 6: Qualitative results on KITTI 2015 test set. From left: left stereo input image, disparity prediction, error map.

in Fig. 5. As can be seen, our EdgeStereo generates finer edge details, compared with the edge map output from HED_β without joint learning. We believe that the geometric knowledge that disparity network has learned can boost highlighting the edge contours, for example, jump in disparity always corresponds to strong image gradients and edges.

5 Conclusion

In this work, we first propose an one-stage stereo network CP-RPN, in which multi-scale context cues are encoded explicitly and all steps in stereo pipeline are integrated for joint optimization. Next we integrate our CP-RPN with a proposed edge detection network HED_β into a multi-task architecture EdgeStereo. Experimental results show that proposed EdgeStereo achieves state-of-the-art performance on two public stereo benchmarks. In addition, both stereo matching task and edge detection task get better after the multi-task learning.

References

1. Achtelek, M., Bachrach, A., He, R., Prentice, S.: Stereo vision and laser odometry for autonomous helicopters in gps-denied indoor environments. *SPIE* (2009)
2. Arbelaez, P., Maire, M., Fowlkes, C., Malik, J.: Contour detection and hierarchical image segmentation. *TPAMI* (2011)
3. Bengio, Y., Louradour, J., Collobert, R., Weston, J.: Curriculum learning. In: *ICML*. pp. 41–48 (2009)
4. Bleyer, M., Rother, C., Kohli, P., Scharstein, D., Sinha, S.: Object stereojoint stereo matching and object segmentation. In: *CVPR*. pp. 3081–3088 (2011)
5. Canny, J.: A computational approach to edge detection. In: *TPAMI* (1986)
6. Chen, L.C., Papandreou, G.: Deeplab: Semantic image segmentation with deep convolutional nets, atrous convolution, and fully connected crfs. *TPAMI* (2016)
7. Chen, Z., Sun, X., Wang, L., Yu, Y., Huang, C.: A deep visual correspondence embedding model for stereo matching costs. In: *ICCV*. pp. 972–980 (2015)
8. Cheng, J., Tsai, Y.H., Wang, S., Yang, M.H.: Segflow: Joint learning for video object segmentation and optical flow. In: *ICCV*. pp. 686–695 (2017)
9. Dollár, P., Appel, R., Belongie, S., Perona, P.: Fast feature pyramids for object detection. *TPAMI* 36(8), 1532–1545 (2014)
10. Geiger, A., Lenz, P., Urtasun, R.: Are we ready for autonomous driving? the kitti vision benchmark suite. In: *CVPR*. pp. 3354–3361 (2012)
11. Gidaris, S., Komodakis, N.: Detect, replace, refine: Deep structured prediction for pixel wise labeling. In: *CVPR*. pp. 5248–5257 (2017)
12. Godard, C., Mac Aodha, O., Brostow, G.J.: Unsupervised monocular depth estimation with left-right consistency. In: *CVPR* (2017)
13. Guney, F., Geiger, A.: Displets: Resolving stereo ambiguities using object knowledge. In: *CVPR*. pp. 4165–4175 (2015)
14. He, K., Zhang, X., Ren, S., Sun, J.: Deep residual learning for image recognition. In: *CVPR*. pp. 770–778 (2016)
15. Hirschmuller, H.: Accurate and efficient stereo processing by semi-global matching and mutual information. In: *CVPR*. pp. 807–814 (2005)
16. Jaderberg, M., Simonyan, K., Zisserman, A., et al.: Spatial transformer networks. In: *NIPS* (2015)
17. Jia, Y., Shelhamer, E., Donahue, J., Karayev, S., Long, J., Girshick, R.: Caffe: Convolutional architecture for fast feature embedding. In: *ACMMM* (2014)
18. Kendall, A., Martirosyan, H., Dasgupta, S., Henry, P., Kennedy, R.: End-to-end learning of geometry and context for deep stereo regression. *CVPR* (2017)
19. Kingma, D.P., Ba, J.: Adam: A method for stochastic optimization. *arXiv preprint arXiv:1412.6980* (2014)
20. Krizhevsky, A., Sutskever, I., Hinton, G.E.: Imagenet classification with deep convolutional neural networks. In: *NIPS*. pp. 1097–1105 (2012)
21. Lin, T.Y., Dollár, P., Girshick, R., He, K., Hariharan, B., Belongie, S.: Feature pyramid networks for object detection. In: *CVPR* (2017)
22. Liu, Y., Lew, M.S.: Learning relaxed deep supervision for better edge detection. In: *CVPR*. pp. 231–240 (2016)
23. Liu, Y., Cheng, M.M., Hu, X., Wang, K., Bai, X.: Richer convolutional features for edge detection. In: *CVPR*. pp. 5872–5881 (2017)
24. Long, J., Shelhamer, E., Darrell, T.: Fully convolutional networks for semantic segmentation. In: *CVPR*. pp. 3431–3440 (2015)

25. Luo, W., Schwing, A.G., Urtasun, R.: Efficient deep learning for stereo matching. In: CVPR. pp. 5695–5703 (2016)
26. Mao, J., Xiao, T.: What can help pedestrian detection? In: CVPR (2017)
27. Mayer, N., Ilg, E., Hausser, P., Fischer, P., Cremers, D., Dosovitskiy, A., Brox, T.: A large dataset to train convolutional networks for disparity, optical flow, and scene flow estimation. In: CVPR. pp. 4040–4048 (2016)
28. Menze, M., Geiger, A.: Object scene flow for autonomous vehicles. In: CVPR. pp. 3061–3070 (2015)
29. Mottaghi, R., Chen, X., Liu, X., Cho, N.G., Lee, S.W.: The role of context for object detection and semantic segmentation in the wild. In: CVPR (2014)
30. Pang, J., Sun, W., Ren, J., Yang, C., Yan, Q.: Cascade residual learning: A two-stage convolutional neural network for stereo matching. In: ICCV Workshop on Geometry Meets Deep Learning. vol. 3 (2017)
31. Ren, S., He, K., Girshick, R., Sun, J.: Faster r-cnn: Towards real-time object detection with region proposal networks. In: NIPS. pp. 91–99 (2015)
32. Scharstein, D., Hirschmüller, H., Kitajima, Y., Krathwohl, G., Nešić, N.: High-resolution stereo datasets with subpixel-accurate ground truth. In: GCPR (2014)
33. Scharstein, D., Szeliski, R.: A taxonomy and evaluation of dense two-frame stereo correspondence algorithms. *IJCV* 47(1-3), 7–42 (2002)
34. Schmid, K., Tomic, T., Ruess, F., Hirschmüller, H., Suppa, M.: Stereo vision based indoor/outdoor navigation for flying robots. In: IROS. pp. 3955–3962 (2013)
35. Seki, A., Pollefeys, M.: Patch based confidence prediction for dense disparity map. In: BMVC (2016)
36. Seki, A., Pollefeys, M.: Sgm-nets: Semi-global matching with neural networks. In: CVPR. pp. 21–26 (2017)
37. Shaked, A., Wolf, L.: Improved stereo matching with constant highway networks and reflective confidence learning. In: ICCV (2017)
38. Xie, S., Tu, Z.: Holistically-nested edge detection. In: ICCV. pp. 1395–1403 (2015)
39. Yamaguchi, K., McAllester, D., Urtasun, R.: Efficient joint segmentation, occlusion labeling, stereo and flow estimation. In: ECCV. pp. 756–771 (2014)
40. Yu, L., Wang, Y., Wu, Y., Jia, Y.: Deep stereo matching with explicit cost aggregation sub-architecture. *AAAI* (2018)
41. Zbontar, J., LeCun, Y.: Stereo matching by training a convolutional neural network to compare image patches. *JMLR* 17(1-32) (2016)
42. Zhang, L., Seitz, S.M.: Estimating optimal parameters for mrf stereo from a single image pair. *TPAMI* 29(2), 331–342 (2007)
43. Zhao, H., Shi, J., Qi, X., Wang, X., Jia, J.: Pyramid scene parsing network. In: CVPR. pp. 2881–2890 (2017)
44. Zhong, Y., Dai, Y., Li, H.: Self-supervised learning for stereo matching with self-improving ability. *CVPR* (2017)